

## Applications of Low Energy Astroparticle Simulations on HPC and Cloud Infrastructures

Hernán Asorey,<sup>a</sup> Y. Domínguez,<sup>b</sup> R. Mayo-García,<sup>c,\*</sup> L. Miranda,<sup>d</sup> L. A. Núñez,<sup>e</sup> O. Núñez-Chongo,<sup>c,f</sup> A. Pardo-Díaz,<sup>c</sup> A. J. Rubio-Montero,<sup>c</sup> C. Sarmiento-Cano,<sup>e</sup> I. Sidelnik,<sup>a</sup> M. Suárez-Durán<sup>g</sup> and A. Taboada<sup>a</sup> for the LAGO collaboration

<sup>a</sup>Comisión Nacional de Energía Atómica (CNEA), Centro Atómico Bariloche, Av. E. Bustillo 9500, San Carlos de Bariloche, Argentina.

<sup>b</sup>East African Institute for Fundamental Research (ICTP-EAIFR), KIST2 Building CST, Nyarugenge Campus, University of Rwanda, Kigali, Rwanda.

<sup>c</sup>CIEMAT, Av. Complutense 40, Madrid, Spain.

<sup>d</sup>Universidad EAFIT, Carrera 19 #12-70, Megacentro Pinares, Pereira, Colombia.

<sup>e</sup>Universidad Industrial de Santander, Carrera 27 #9-10, Bucaramanga, Santander, Colombia.

<sup>f</sup>Universidad Carlos III de Madrid, Av. de la Universidad 30, Leganés, Madrid, Spain.

<sup>g</sup>Universidad de Pamplona, km 1 Vía Bucaramanga, Pamplona, Norte de Santander, Colombia.

E-mail: [hernanasorey@cnea.gov.ar](mailto:hernanasorey@cnea.gov.ar), [rafael.mayo@ciemat.es](mailto:rafael.mayo@ciemat.es)

The Latin American Giant Observatory (LAGO) is an extensive network of water Cherenkov detectors spread across Latin America, functioning as an astroparticle observatory. With its broad range of altitudes and geomagnetic rigidity cut-offs, the primary focus of LAGO's scientific program is to study space weather, climate phenomena, and high-energy astrophysical transients from ground level. To bolster these programs, the comprehensive simulation framework of ARTI and onedataSim was developed. This framework enables the calculation of the total secondary particle flux and the corresponding signals expected in various types of detectors operating anywhere in the world. It also incorporates the effects of real-time atmospheric and geomagnetic conditions, both secular and disturbed. These tools harness the expanding computational capabilities of high-performance computing facilities and cloud-based computing environments. By integrating these tools and infrastructures, we have managed to extend the total integration times of the background flux and the energy range of atmospheric neutrons. In this contribution, we illustrate how this intricate simulation sequence aids in achieving LAGO's scientific objectives. We also explore other applications, such as estimating the expected dose on board commercial flights, simulating the muon flux for muography studies, determining the distribution of neutrons in nuclear and medical facilities, and estimating the rate of errors produced by atmospheric neutrons in the upcoming generation of exascale supercomputing centers worldwide.

The 38th International Cosmic Ray Conference (ICRC2023)  
26 July – 3 August, 2023  
Nagoya, Japan



\*Speaker

## 1. Introduction

The Latin American Giant Observatory (LAGO) [1] is a comprehensive cosmic ray observatory, featuring a network of water Cherenkov detectors (WCD) distributed across Latin America. This network encompasses a wide range of geomagnetic rigidity cut-offs and atmospheric absorption/reaction levels [2]. The LAGO WCD is designed for robustness and simplicity, with integrated devices for time synchronization, autonomous operation, onboard data analysis, and automated data handling [1]. Designed to measure the temporal evolution of the atmospheric reaction to the cosmic ray flux at ground level, LAGO's detection network focuses on high energy phenomena, space weather, and atmospheric radiation at ground level [1]. The LAGO Collaboration, a collective of over 30 institutions from eleven Ibero-American countries, operates the observatory.

Currently, operational are ten WCDs, with eleven more anticipated to start operation soon. The network's geographical distribution allows for simultaneous measurements at different rigidity cut-offs, enabling LAGO to provide near-real-time information on disturbances induced by interplanetary transients and long-term space weather phenomena [3]. Each LAGO WCD features a plastic tank filled with purified water, and one to four top-mounted large photomultiplier tubes (PMT) that collect the Cherenkov light produced by ultra-relativistic particles. The PMT signals are shaped and digitized by advanced onboard electronics, which also monitor telemetry variables and local atmospheric conditions.

The LAGO project covers a wide spectrum of activities, from detector installation and operation to data transfer methods from remote locations. It includes comprehensive simulation sequences [4], tailored data analysis techniques [3], data curation and preservation [5], and the design of new experiments for participating universities.

## 2. Precise simulations of the atmospheric background radiation

The primary source of background radiation is the constant influx of secondary particles generated through the interaction of primary cosmic rays (CR) with the atmosphere. Accurately simulating the development of Extensive Air Showers (EAS) and tracking secondary particles is a computationally intensive task. CORSIKA is the most widely used and validated tool developed for this purpose. It allows for selecting the interaction models, specific atmospheric models, the configuration of the local Earth's magnetic field (EMF) components, and setting different observation level altitudes.

The atmospheric radiation is a result of the convolution of the cascade development of billions of cosmic rays that simultaneously impinge the Earth's atmosphere. When forecasting the expected background radiation at any specific location worldwide, particularly under distinct and variable EMF atmospheric conditions, these factors play a crucial role. These elements directly affect the number of primary particles impinging on the Earth's atmosphere and the cascade evolution, and so, the subsequent flux of secondary particles at ground level. LAGO has created ARTI [4], a toolkit engineered to compute and analyze the total background flux of secondary particles produced by the atmospheric reaction to the primary flux of GCR. It is a computational publicly available tool that combines CORSIKA, Magnetocsmic, and Geant4 with its own custom control and data

analysis codes. The ground-level flux predicted by ARTI has been cross-checked and validated with measurements taken at various astroparticle observatories.

The accurate modelling of the anticipated atmospheric flux is contingent upon the statistical significance of the calculated secondary flux at ground level. This is achieved by extending the time integration of the flux sufficiently to prevent it from being dominated by expected statistical fluctuations [1]. For instance, a typical calculation of the expected number of secondary particles per square meter per day at a high-latitude site requires the computation of approximately  $10^9$  primary EAS. To manage this, ARTI has been incorporated into a new application, onedataSim [5], which can be effortlessly deployed and executed on high-performance computing (HPC) clusters and cloud-based environments, whether they are public, such as AWS or Google Cloud, or federated, like the European Open Science Cloud (EOSC).

The onedataSim architecture is designed with three core stages of computation, each represented by a Docker image: S0, S1, and S2 [5]. The S0 stage generates raw data from CORSIKA simulations managed by ARTI. The S1 stage then transforms this raw data into a new catalog of analyzed data using ARTI's analysis tools. The final stage, S2, simulated the detector response and expected signals at ground level by processing the output from the S1 stage, which is done using a highly configurable Geant4 model of the LAGO WCD, constructed with MEIGA, a framework designed initially for muography applications [6].

OnedataSim generates data and metadata using standardized schemas rooted in linked data principles. The language syntax employed is JSON-LD 1.1 (W3C), the primary vocabulary is DCAT-AP2 (European Commission), and the newly introduced LAGO vocabulary is a re-profile of DCAT-AP2. This method of data organization, structured into catalogs and datasets, ensures that each generated file is treated as the minimal dataset for data-linking and processing. Collections of related files are grouped into a catalog, which is assigned unique Persistent Identifiers (PIDs) provided by B2HANDLE and harvested by the B2FIND services. The resulting data are then transferred and stored in cloud-storage services offered by the EGI-DataHub. The Data Management Plan (DMP) serves as the primary resource that integrates all the requirements for implementing the Open Science paradigm within LAGO [7]. It guarantees adherence to the Findability, Accessibility, Interoperability, and Reusability (FAIR) principles for the results and establishes the format of the data and metadata, as well as the protocol for generating, storing, and accessing the results [5].

### 3. Astroparticle and Social-prompted Applications

Implementing ARTI and onedataSim has opened up new possibilities by leveraging increased computing power. We have calculated the total 1- to 7-day flux with the minimum available energy cutoff, considering local atmospheric effects using monthly averaged Global Data Assimilation System atmospheric profiles and directional and time-dependent local geomagnetic rigidity cutoffs.

In Fig. 1 we show the expected momentum of secondary particles at ground level for a new site in Mendoza, Argentina. Simulations were performed using local atmospheric monthly average profiles for 2022, to detect potential seasonal effects on the total flux. A variation of 2-4% in the flux of neutrons with  $E_n > 20$  MeV at ground level was observed between summer and winter. Given the proximity to the Andean range, this site provides a range of observation altitudes above sea level (asl) within a short distance. So, the expected flux for each month was also simulated

from 875 m asl up to 5,000 m asl. To enhance the statistical significance of these results, a 4-day equivalent flux was simulated for each altitude and atmospheric profile, utilizing the cloud and HPC implementations provided by the new ARTI/onedataSim [4, 5].

ARTI calculate more than the expected background. It can also predict the expected flux of secondary particles during high-energy astrophysics events like gamma-ray bursts [3]. ARTI and MEIGA drive a new calibration method to measure deviations from the expected value for muon lifetime in water and characterize the resulting electron's Michel spectrum. It provides a promising tool for obtaining the signal-to-deposited-energy calibration constant and improving the noise-to-signal separation ratio at the WCD [8]. We also implement the simulated detector signals from ARTI-MEIGA to train deep-learning methods for pulse identification at the single-particle level on measured data at the BRC LAGO site.

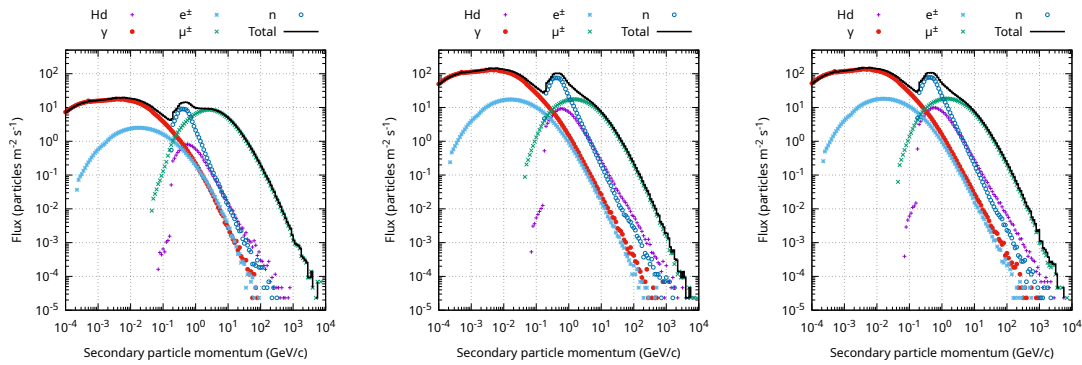


**Figure 1:** The momentum spectrum of the anticipated flux of secondary particles at a new LAGO site (TUN), currently under development in the province of Mendoza, Argentina, is presented. The impact of atmospheric interactions is evident when comparing the expected flux in January at 875 m asl (left), with the corresponding flux at 4500 m asl during the same season (center). Furthermore, subtle yet discernible differences (+3.7%) can be observed between the summer and winter flux (right), particularly for the neutron flux at the same altitude.

ARTI/onedataSim and MEIGA have also been used for the development of socially-triggered applications. For instance, we have recently reported the most statistically significant flux of high-energy muons expected at the ANDES subterranean laboratory [5]. This corresponds to 1.5 years of the expected flux of very-high-energy muons ( $E_\mu > 800$  MeV), with energy capable to reach the ANDES lab under 1650 m of rock. It has been also used for the MuTe muographier characterization in Colombia, for the design of new muography modular detectors in Argentina, and for evaluating the muon transport in rock for mining prospecting applications [6].

### 3.1 ACORDE: A Comprehensive Calculation of Atmospheric Radiation Dose Estimation During Flights

Leveraging the robust foundations provided by CORSIKA, Geant4, and the enhancements introduced by the ARTI framework, we developed ACORDE (Application CODE for the Radiation Dose Estimation) [9]. This tool is designed to calculate the radiation dose absorbed by aircraft crew and passengers during commercial flights. The ACORDE workflow begins with the identification of the flight and the extraction of relevant information from public databases. The flight is then

divided into three main stages: takeoff, cruise, and landing. The cruise stage is further divided into segments of varying duration depending on the total duration of the flight. Each segment is defined by a four-dimensional vector consisting of geographic coordinates (latitude, longitude, and altitude above sea level) and the UTC time. Once the waypoints have been obtained and the track has been segmented, the local atmospheric profile corresponding to each waypoint for that particular moment is extracted, as well as the instantaneous value of the EMF and the directional rigidity-cutoff tensor. Once all this data is gathered, the expected atmospheric radiation is calculated at each waypoint.

In Figure 2, three main aspects of ACORDE's methodology are illustrated. In the left panel, the real track of the IB3270 flight that took place on Nov, 16th, 2021 is shown, as well as the waypoints identified in the cruise stage of the flight. Minor yet significant variations can be seen between the different local profiles (center panel). Furthermore, these differences become substantially larger when each of these profiles is compared with the standard atmospheric profile: at  $h=37,000$  ft, the difference between local and standard profile is off  $12.5 \text{ g cm}^{-2}$ , equivalent to approximately 1.3 kPa (around 5%). Such differences can even exceed 15% for flights near the polar regions [2].

The third stage of ACORDE consists of a Geant4 model of the fuselages of the Airbus A320/A350 aircraft. It is constructed as a succession of three concentric and hollow cylinders. Within this cabin, a simplified anthropomorphic water-based phantom model based on the ICRP-110 Recommendations is placed. All the secondary particles expected at each waypoint are propagated through this model, and the corresponding absorbed, equivalent and effective doses are calculated following the ICRP-103 Recommendations. Finally, the total dose is obtained by integrating the respective doses at each waypoint, including the takeoff and landing phases.

We applied this procedure for 324 flights registered during 2021-22, which were classified into three categories based on their cruise stage duration: short (less than 2 hours), intermediate (less than 4 hours), and long (more than 4 hours). We compare ACORDE's results with the corresponding doses calculated using the extensively adopted tool CARI7-A [10]. Our findings show that ACORDE's dose estimation was, on average, systematically larger than the corresponding CARI7-A effective dose, especially for long flights. However, the observed absolute and average differences between the effective dose calculated with ACORDE and CARI7-A were compatible with zero within the systematic error bars in all three studied groups. However, this is not the case when considering geomagnetic disturbances. For these cases, the dose reported by ACORDE could be significantly larger than the corresponding CARI7-A dose.

### 3.2 Low-energy atmospheric neutron flux

The production of neutrons by cosmic rays within Earth's atmosphere is a topic of profound significance due to its potential applications in various fields. The components and the profile of the atmosphere play important roles in the final distribution of neutrons at ground level. The accurate calculation of neutron flux at a specific location is of considerable importance due to its direct correlation with potential computer failures. This concern is particularly acute in the era of exascale computing, where the risks associated with neutron and other atmospheric radiation are intensifying as computational power increases. As a result, the expected mean time between failures (MTBF) is anticipated to decrease due to the effects of this radiation. Energy deposition in semiconductors leads to various problems, with single-event effects (SEE) being the most impactful. Two types of SEE are typically studied: soft errors, also known as single event upsets (SEU) in

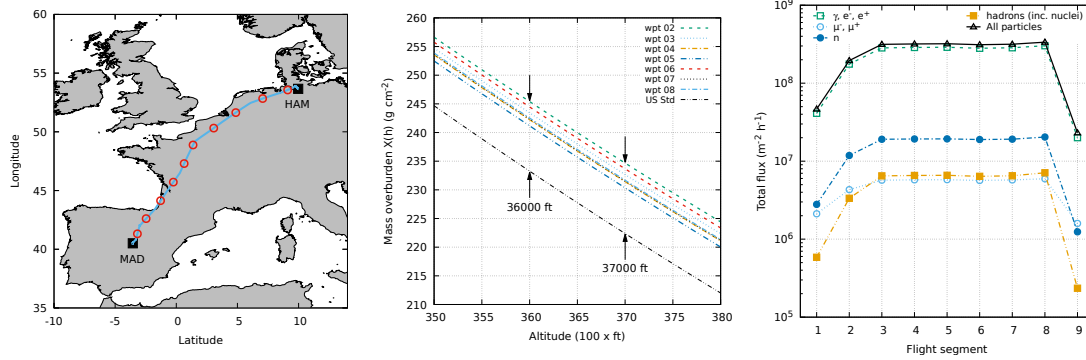


**Figure 2:** Left: the actual flight path (depicted in light blue) of flight IB3270 from MAD to HAM on 11/16/2021 is shown, with the start and end of the cruise stage determined by ACORDE. The points where the dose was calculated are marked with red circles. Center: the atmospheric mass overburden  $X(h)$  as a function of altitude  $h$  for the seven cruise segments of flight IB3270 at flight altitude is displayed. This data was derived from atmospheric profiles from the GDAS database. The observed difference between the local and US standard atmospheric profiles at flight altitudes is approximately 1.3 kPa (around 5%). Right: the evolution of the integrated flux throughout the flight is shown for different components as well as for the total flux.

the literature, and hard (or catastrophic) errors, such as the single event latch-up. Among these, Silent Errors (SE) are considered the most dangerous due to their stealthy nature. These errors occur during program execution but do not cause the program to crash or produce an immediately observable incorrect result.

The effective SE cross-section  $\sigma_{\text{SE}}$ , that is, the number of silent errors expected in a specific piece of hardware exposed to a given neutron flux, has been experimentally determined for several commercially available systems [11]. By combining these types of measurements with the expected flux of neutrons at a certain location, it is possible to create a decision-making tool for the administrators of exascale supercomputers. To achieve this, we extracted atmospheric profiles from the GDAS database and averaged them to obtain the atmospheric conditions for each month of 2020 at each of the proposed 23 sites where exascale centers will be installed worldwide. We then used ARTI to calculate the expected flux of high-energy neutrons and their seasonal variations at each exascale supercomputing center. As an example of this calculation, the left panel of figure 3 shows the total flux as well as the independent components flux for each month at the National Supercomputing Center in Wuxi (NSCW), China, at 10 m above sea level. In this case, the flux of electromagnetic particles is significantly reduced due to air absorption in the denser layers of the lower atmosphere, and thus, the barometric modulation in Wuxi for the total flux is not as large as for neutrons. However, the anticorrelation observed for the neutron flux is extremely remarkable, as can be seen in the central panel of Fig. 3. By repeating this procedure at every site, we obtained the local neutron reference flux and the corresponding barometric pressure coefficients for neutrons. These coefficients correspond to the relative change in the expected flux in different energy ranges when the local atmospheric pressure changes by  $\pm 1$  hPa. This information allows for the estimation of the expected flux of neutrons under different atmospheric conditions and the evaluation of the corresponding failure in time (FIT) rates of silent errors due to high-energy neutrons. As an example,



the corresponding MTBF originated by SE for the Titan supercomputer at the Oak Ridge National Laboratory (ORNL), could be approximately 23 hours due to a pressure drop of  $-5$  hPa [12].

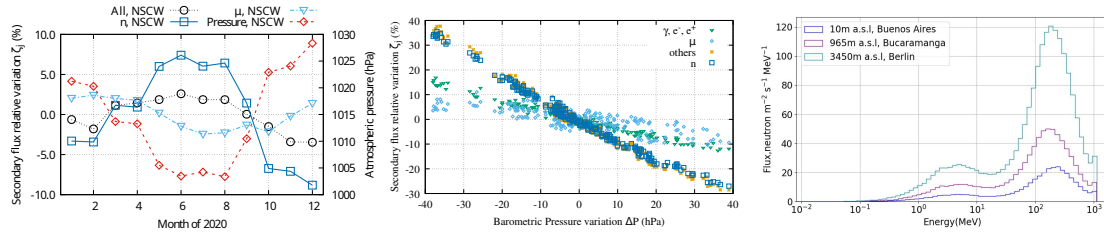


**Figure 3:** Anticipated relative flux variations for neutrons (blue solid line and empty squares), muons (light blue dot-dashed line and empty triangles), and all secondary particles (black dotted line and empty circles). The local atmospheric pressure at ground level is also depicted (red dashed line and empty rhombus, right axis). These data points are presented for each month of 2020 at the National Supercomputing Center in Wuxi (NSCW, sea level, left). The anti-correlation is evident at all the studied sites, except for muons, as expected. This is particularly pronounced for the neutron flux, as can be seen in the central panel for all the simulated sites. In the right panel, the neutron flux extended down to the thermal energy range is shown for three different LAGO sites.

For studies of this nature, it would be beneficial to expand the current energy range for neutrons down to the thermal (meV) energy range [13]. We extended the current CORSIKA-FLUKA implementation by incorporating a Geant4 Linsley-based model of the atmospheric profile near the ground and overlapping it with CORSIKA simulations, after determining that the overlapping region should be 2,000 m above the ground level. Using a layered atmospheric model in Geant4, we injected secondary particles from ARTI while preserving their energy and direction, allowing us to extend the neutron energy range to meV, as can be seen in the right panel of Fig. 3. Ongoing investigations are focused on improving our models and the Geant4 physics models.

#### 4. Conclusions and future work

This paper has presented a comprehensive overview of the advancements in the simulation of atmospheric background radiation and its various applications. The development of tools such as ARTI and onedataSim has significantly enhanced our ability to simulate the development of extensive air showers and the propagation of secondary particles. These tools have been instrumental in studying the effects of space weather phenomena at ground level, predicting the expected background radiation at specific locations worldwide, and simulating detector signals.

Furthermore, these tools have been used in socially-prompted applications such as the development of safer methods for the detection of improvised explosive devices, muography for mining prospecting, and even in the agriculture sector. The development of ACORDE, a tool designed to calculate the radiation dose absorbed by aircraft crew and passengers during commercial flights, is another notable application.

The study of low-energy atmospheric neutron flux has also been enhanced by these tools. The accurate calculation of neutron flux at a specific location is of considerable importance due to its direct correlation with potential computer failures, especially in the era of exascale computing. The development of a decision-making tool for the administrators of exascale supercomputers,

which enables them to determine in advance which mitigation methodologies need to be applied to overcome silent errors, depending on the forecasted neutron flux in a specific period of the year, is a significant achievement. Future work will focus on improving these tools and exploring new applications of social interest.

### Acknowledgements

This work has been partially carried out on the ITeDA cluster, we thank A.P.J. Sedosky-Croce for his continuous support. This work has been partially funded by MINCIENCIAS under project 82242 of call 890 of 2020, managed through the ICETEX contract 2022-0718.

### References

- [1] I. Sidelnik and H. Asorey. Lago: The latin american giant observatory. *Nuclear Instruments and Methods A*, 876: 173–175, 2017-12. doi: 10.1016/j.nima.2017.02.069.
- [2] S. Dasso et al. A project to install water-cherenkov detectors in the antarctic peninsula as part of the lago detection network. In *Proceedings of the 34th International Cosmic Ray Conference (ICRC2015)*, page 105, 2015. doi: 10.22323/1.236.0105.
- [3] Christian Sarmiento-Cano, Hernán Asorey, Jose Sacahui, Luis Otiniano, and Iván Sidelnik. The latin american giant observatory (lago) capabilities for detecting gamma ray bursts. In *Proceedings of the 37th International Cosmic Ray Conference (ICRC2021)*, page 929, 2021. doi: 10.22323/1.395.0929.
- [4] C. Sarmiento-Cano et al. The arti framework: cosmic rays atmospheric background simulations. *The European Physical Journal C*, 82:1019, 2022. doi: 10.1140/epjc/s10052-022-10883-z.
- [5] A. J. Rubio-Montero et al. A novel cloud-based framework for standardized simulations in the latin american giant observatory (lago). In *2021 Winter Simulation Conference (WSC)*, volume 2021, pages 1–12, 2021. doi: 10.1109/WSC52266.2021.9715360.
- [6] A. Taboada et al. Meiga, a dedicated framework used for muography applications. *Journal of Advanced Instrumentation in Science*, 2022, 2022. doi: 10.31526/JAIS.2022.266.
- [7] A. Calatrava et al. A survey of the european open science cloud services for expanding the capacity and capabilities of multidisciplinary scientific applications. *Computer Science Review*, 49:100571, 2023. doi: 10.1016/j.cosrev.2023.100571.
- [8] L. Otiniano et al. Measurement of the muon lifetime and the michel spectrum in the lago water cherenkov detectors as a tool to enhance the signal-to-noise ratio. *Nuclear Instruments and Methods A*, accepted, 2023.
- [9] H. Asorey et al. Acorde: A new application for estimating the dose absorbed by passengers and crews in commercial flights. *Applied Radiation and Isotopes*, 196, 2023. doi: 10.1016/j.apradiso.2023.110752.
- [10] K. Copeland. Cari-7a: Development and validation. *Radiation Protection Dosimetry*, 175:419–431, 2017-01. doi: 10.1093/rpd/ncw369.
- [11] A. Bustos et al. Response of hpc hardware to neutron radiation at the dawn of exascale. *The Journal of Supercomputing*, 79:13817–13838, 2023. doi: 10.1007/s11227-023-05199-y.
- [12] H. Asorey and R. Mayo-García. Calculation of the high-energy neutron flux for anticipating errors and recovery techniques in exascale supercomputer centres. *The Journal of Supercomputing*, 79:8205–8235, 2022. doi: 10.1007/s11227-022-04981-8.
- [13] Ralph Engel et al. Neutron production in extensive air showers. In *Proceedings of the 37th International Cosmic Ray Conference (ICRC2021)*, page 492, 2021.



**Full Authors List: The LAGO Collaboration**

V. Agosín<sup>30</sup>, A. Alberto<sup>3</sup>, C. Alvarez-Ochoa<sup>15</sup>, J. Araya<sup>30</sup>, R. Arceo<sup>15</sup>, O. Areso<sup>12</sup>, L.H. Arnaldi<sup>2</sup>, H. Asorey<sup>2</sup>, M. Audelo<sup>8</sup>, M.G. Ballina-Escobar<sup>18</sup>, D. Blanco<sup>23</sup>, M. Bonilla<sup>15</sup>, K.S. Caballero-Mora<sup>15</sup>, R. Caiza<sup>7</sup>, R. Calderón-Ardila<sup>13</sup>, A.C. Fauth<sup>27</sup>, A. Carramiñana-Alonso<sup>14</sup>, E. Carrera-Jarrín<sup>26</sup>, C. Castromonte<sup>25</sup>, D. Cazar<sup>26</sup>, C. Gutierrez<sup>5</sup>, V. Clarizio<sup>22</sup>, D. Cogollo<sup>28</sup>, D. Coloma-Borja<sup>26</sup>, R. Conde<sup>1</sup>, J. Cotzomi<sup>1</sup>, S. Dasso<sup>12,5</sup>, A. Albuquerque<sup>28</sup>, J.H.A.P. Reis<sup>27</sup>, H. De-León<sup>15</sup>, D. Domínguez<sup>7</sup>, J.A. Durán<sup>23</sup>, M. Echiburru<sup>20</sup>, M. González<sup>13</sup>, M. Gómez-Berisso<sup>2</sup>, J. Grisales-Casadiegos<sup>22</sup>, A.M. Gulisano<sup>12,6,11</sup>, J. Helo<sup>16</sup>, C. Huanca<sup>23</sup>, J.E. Ise<sup>10</sup>, M.A. Leigui-de-Oliveira<sup>29</sup>, V.P. Luzio<sup>29</sup>, F. Machado<sup>25</sup>, D. Manriquez<sup>30</sup>, A. Martínez-Méndez<sup>22</sup>, R. Mayo-García<sup>3</sup>, L.G. Mijangos<sup>21</sup>, P. Miranda<sup>23</sup>, M.G. Mischieri<sup>28</sup>, M.G. Molina<sup>10</sup>, O.G. Morales-Olivares<sup>15</sup>, E. Moreno-Barbosa<sup>1</sup>, P. Muñoz<sup>16</sup>, C. Nina<sup>23</sup>, L.A. Núñez<sup>22</sup>, L. Otiniano<sup>4</sup>, R. Pagán-Muñoz<sup>3</sup>, L. Palma<sup>16</sup>, R. Parra<sup>9</sup>, J. Peña-Rodríguez<sup>22</sup>, M. Pereira<sup>12</sup>, H. Perez<sup>18</sup>, J. Pisco-Guabave<sup>22</sup>, E. Ponce<sup>1</sup>, R. Quispe<sup>23</sup>, M. Raljevic<sup>23</sup>, M. Ramelli<sup>12</sup>, L.T. Rubinstein<sup>12</sup>, A.J. Rubio-Montero<sup>3</sup>, J.R. Sacahui<sup>18</sup>, H. Salazar<sup>1</sup>, J. Samanes<sup>4</sup>, N.A. Santos<sup>5</sup>, C. Sarmiento-Cano<sup>22</sup>, I. Sidelnik<sup>2</sup>, D. Sierra-Porta<sup>22</sup>, O. Soto<sup>16</sup>, L. Stuaní<sup>28</sup>, M. Suárez-Durán<sup>17</sup>, M. Subieta<sup>23</sup>, A. Taboada-Núñez<sup>13</sup>, J. Terrazas<sup>23</sup>, R. Ticona<sup>23</sup>, T. Torres-Peralta<sup>10</sup>, P. Ulloa<sup>16</sup>, Z.R. Urrutia<sup>21</sup>, N. Vásquez<sup>7</sup>, A. Vázquez-Ramírez<sup>22</sup>, J. Vega<sup>4</sup>, P. Vega<sup>16</sup>, A. Vega<sup>19</sup>, A. Vesga-Ramírez<sup>13</sup>, L. Villaseñor-Cendejas<sup>24</sup>, V.R. Ribeiro<sup>28</sup> and R. Wiklich-Sobrinho<sup>29</sup>

<sup>1</sup>Benemérita Universidad Autónoma de Puebla. <sup>2</sup>Centro Atómico Bariloche (CNEA/CONICET/IB). <sup>3</sup>Centro de Investigaciones Energéticas, Medioambientales y Tecnológicas. <sup>4</sup>Comisión Nacional de Investigación y Desarrollo Aeroespacial. <sup>5</sup>Departamento de Ciencias de la Atmósfera y los Océanos, Facultad de Ciencias Exactas y Naturales, Universidad de Buenos Aires. <sup>6</sup>Departamento Física, Facultad de Ciencias Exactas y Naturales, Universidad de Buenos Aires, Argentina (DFUBA). <sup>7</sup>Escuela Politécnica Nacional. <sup>8</sup>Escuela Superior Politécnica de Chimborazo. <sup>9</sup>European Southern Observatory (ESO). <sup>10</sup>Facultad de Ciencias Exactas y Tecnología (FACET) – Universidad Nacional de Tucumán (UNT). <sup>11</sup>Instituto Antártico Argentino. <sup>12</sup>Instituto de Astronomía y Física del Espacio, IAFE (UBA-CONICET). <sup>13</sup>Instituto de Tecnologías en Detección y Astropartículas (CNEA, CONICET, UNSAM). <sup>14</sup>Instituto Nacional de Astrofísica, Óptica y Electrónica. <sup>15</sup>Universidad Autónoma de Chiapas. <sup>16</sup>Universidad de La Serena. <sup>17</sup>Universidad de Pamplona. <sup>18</sup>Universidad de San Carlos. <sup>19</sup>Universidad de Valparaíso. <sup>20</sup>Universidad de Viña del Mar. <sup>21</sup>Universidad del Valle de Guatemala. <sup>22</sup>Universidad Industrial de Santander. <sup>23</sup>Universidad Mayor de San Andrés. <sup>24</sup>Universidad Michoacana de San Nicolás de Hidalgo. <sup>25</sup>Universidad Nacional de Ingeniería. <sup>26</sup>Universidad San Francisco de Quito. <sup>27</sup>Universidade Estadual de Campinas. <sup>28</sup>Universidade Federal de Campina Grande. <sup>29</sup>Universidade Federal do ABC. <sup>30</sup>No Affiliation.